JGR Oceans

RESEARCH ARTICLE
10.1029/2018JC013978

Key Points:
- ROV with cameras were employed to study methane bubbles rising in ocean
- Size evolution of rising methane bubbles is reported
- Data from bubble size evolution are applied to shed led light on gas dissolution and mass transfer coefficient

Supporting Information:
- Supporting Information S1
- Data Set S1

Correspondence to:
J. E. Olsen,
jan.e.olsen@sintef.no

Citation:
Olsen, J. E., Krause, D. F., Davies, E. J., & Skjetne, P. (2019). Observations of rising methane bubbles in Trondheimsfjord and its implications to gas dissolution. *Journal of Geophysical Research: Oceans*, *124*. https://doi.org/10.1029/2018JC013978

Received 13 MAR 2018
Accepted 10 FEB 2019
Accepted article online 13 FEB 2019

Observations of Rising Methane Bubbles in Trondheimsfjord and Its Implications to Gas Dissolution

J. E. Olsen[1], D. F. Krause[2], E. J. Davies[2], and P. Skjetne[1]

[1]SINTEF Industry, Trondheim, Norway, [2]SINTEF Ocean, Trondheim, Norway

Abstract Gas dissolution reduces the release of methane to the atmosphere from subsea sources. Being able to predict and assess the methane flux to the atmosphere requires knowledge on gas dissolution and mass transfer. This can be obtained by studying the size evolution of bubbles rising in water. New data of bubble size evolution have been obtained by releasing, tracking, and filming methane bubbles with an ROV in the Trondheimsfjord from depths varying between 100 and 300 m. Released bubbles had an initial diameter between 5 and 7 mm and were tracked until they reached a diameter of roughly 2 mm. The new data were compared against theory, applying established correlations for the mass transfer coefficient. There was an inconsistency between experiment and theory. Thus, new correlations for the mass transfer are proposed. The new correlations are consistent with both the new experiments and previously published experiments. They indicate that the conditions in the ocean can be labeled as partly contaminated with respect to mass transfer.

Plain Language Summary Methane bubbles released from the ocean can reach the atmosphere and affect the methane concentration in the atmosphere. Methane is a potent greenhouse gas and highly combustible. How much gas enters the atmosphere depends on how much gas is dissolved in the ocean. The shrinking of bubbles and the development of bubble size are signatures of the gas dissolution. There is a lack of knowledge on methane dissolution in seawater. An experiment outside Trondheim, Norway, has been conducted where an ROV released methane bubbles and recorded images of the bubbles as they rose upward. These images have been analyzed to shed light on gas dissolution.

1. Introduction

When methane is released at the seabed, it travels toward the ocean surface as bubbles where it escapes into the atmosphere unless it is completely dissolved in the ocean. Methane in the atmosphere can have a negative impact on climate and environment since it is a potent greenhouse gas (IPCC, 2013). With increasing sea temperatures there is a growing concern that melting of hydrates below the seabed will increase and release more methane through the seabed (Ruppel & Kessler, 2017). Methane can also be released from gas blowouts which typically cause significantly higher gas concentrations than natural seeps, however over a much shorter time span. The concentration might be sufficient to cause a fire and/or explosion that poses a risk to humans and assets (Olsen & Skjetne, 2016a). Being able to estimate how much gas that escapes into the atmosphere is thus an important input to any risk assessment and impact study. The estimate needs to account for gas dissolution. Gas dissolution from bubbles depends on the mass transfer mechanism, which has been widely studied in freshwater and chemical reactors, but only to a limited degree for bubbles in the ocean (Leifer & Patro, 2002; McGinnis et al., 2006; Rehder et al., 2002, 2009). In this article we try to extend the knowledge on mass transfer between bubbles and seawater.

Gas dissolution and mass transfer is driven by the difference between gas solubility and background gas concentration. It is also proportional to the surface area of the bubbles and the mass transfer coefficient. The mass transfer coefficient represents a species transfer velocity accounting for the diffusive transport mechanism across the interface at which the mass transfer occurs. The coefficient depends among others upon the concentration of surfactants in the ocean. Surfactants tend to immobilize the bubble surface which reduces mass transfer. The effect of surfactants on bubbles has been studied extensively. A substantial summary of this work is provided by Leifer and Patro (2002). Mathematical expressions for the mass transfer coefficient are typically classified as expressions for contaminated, partly contaminated, or clean conditions. Partly

contaminated is a contamination regime where a transitions from contaminated to clean behavior on the drag or mass transfer is observed as the bubble size increases.

Several studies in freshwater have been conducted where the level of contamination has been varied. Takemura and Yabe (1999) performed experiments with CO_2 bubbles rising in a lab-scale bubble column with both clean and contaminated water. Alves et al. (2005) studied bubbles in a downward flowing water column where they maintained a fixed position of air bubbles for observations with various contamination. Recently, Aoki et al. (2015) measured the development of bubble size in a vertical pipe with controlled concentrations of surfactants. All of these studies (and others) document that the concentration of surfactants affects mass transfer. Numerous types of surfactants exist in the ocean. They are mainly the products of biological processes involving phytoplankton (Sabbaghzadeh et al., 2017) and include substances such as polysaccharides and lipids (Leifer & Patro, 2002). Thus, the amount of surfactants in the ocean varies with location, depth, and season (Pakulski & Brenner, 1994) as does the concentration of phytoplankton. Typically, surfactant concentration decreases with depth. However, even small concentrations of surfactants at great depths can be enough for the water to behave as contaminated with respect to mass transfer.

Very few observations and experiments on mass transfer exist which have been conducted in true seawater. The most relevant experiment is the experiment performed by Rehder et al. (2002), which tracked and photographed bubbles released in the ocean outside Monterey with an ROV. Methane bubbles were released between 440 and 840 m of depth. This experiment was later repeated at depths down to 1,500 m (Rehder et al., 2009). Recently, Olsen et al. (2017) performed experiments in a downward flowing column with seawater pumped in to the lab from a depth of 70 m. There are other experiments/observations below the hydrate stability limit (e.g., Rehder et al., 2009; Wang et al., 2016). In these data there are the combined complexity of hydrates and the issue of choice of mass transfer coefficient, but some good observations can be extracted. Also, studies with artificial seawater have been undertaken (Laqua et al., 2016). Artificial seawater will have the correct salinity, but it might be questionable with respect to realistic representation of surfactants.

When replicating the observations of Rehder et al. (2002), a mass transfer coefficient for partly contaminated conditions was applied (McGinnis et al., 2006; Zheng & Yapa, 2002). Due to this, a mass transfer correlation for partly contaminated conditions is widely used in models for bubble plumes in the ocean. The more recent observations made by Olsen et al. (2017) support the use of correlations for contaminated conditions, not partly contaminated. The main differences between these experiments are the geographical location and depth of the seawater and the bubble size. The bubbles studied by Rehder et al. (2002) were larger than 4 mm, while the bubbles studied by Olsen et al. (2017) were smaller than 1 mm. The experiment of Olsen et al. (2017) was also conducted in the lab. Even if seawater was taken from the ocean, it can always be argued that in order to study true conditions, measurements should be performed in the sea. Thus, a field experiment was conducted in Trondheimsfjord outside Trondheim in Norway based on the same principles of Rehder et al. (2002) with an ROV releasing, tracking, and recording images of methane bubbles. The bubbles were released from 100- to 300-m depth. These depths were chosen to focus on the mass transfer coefficient for bubbles without hydrate rim to avoid adding complexity to the issue. Following a theoretical outline of mass transfer, the results of these experiments are presented below.

2. Gas Dissolution and Bubble Size

Bubbles rise in water due to buoyancy. The rise velocity is governed by the force balance on bubbles

$$\dot{\vec{u}}_b = \frac{18\mu}{\rho_b d_b^2}\,\frac{\mathrm{Re}\,C_D}{24}\left(\vec{u}-\vec{u}_b\right) + \vec{g}\,\frac{(\rho_b-\rho)}{\rho_b} \tag{1}$$

where the first term on the right-hand side represents the drag force and the second term represents the buoyancy force. Here u is the velocity, μ is the viscosity, ρ is the density, d is the diameter, Re is the Reynolds number, C_D is the drag coefficient, and g is the gravitational acceleration. Note that a dot above a symbol indicates the time derivate of the quantity represented by the symbol and that subscript b is used for properties of the bubbles. The influence of the background velocity from the water surrounding the bubble can be strong for bubbles originating from gas blowouts. For natural seeps the background velocity is less significant and often neglectable (Leifer & Patro, 2002).

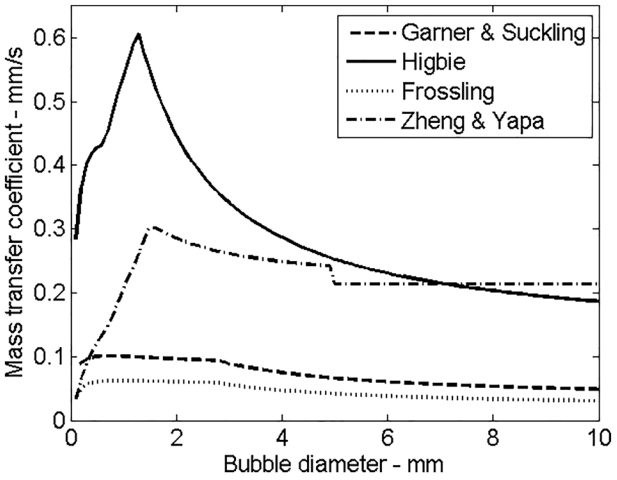

Figure 1. Plots of various mass transfer correlations for clean (Higbie, 1935), partly contaminated conditions (Zheng & Yapa, 2002), and contaminated conditions (Frössling, 1938; Garner & Suckling, 1958).

When buoyancy and drag force are equal in magnitude there is no acceleration on bubbles, $\dot{\vec{u}}_b = \mathbf{0}$, and bubbles rise with a velocity known as the terminal velocity. From equation (1)) and the definition of the Reynolds number we get

$$u_t = \sqrt{\frac{4}{3}\frac{g d_b}{C_D}\frac{\rho - \rho_b}{\rho}} \tag{2}$$

This shows that the bubble rise velocity depends on density, size, and drag coefficient. The drag coefficient is a function of Reynolds and Eotvos numbers and will also vary between bubbles with clean and contaminated interfaces. In the numerical examples shown below the drag correlations of Tomiyama et al. (1998) have been applied. They provided correlations for clean, contaminated, and an intermediate condition named partly contaminated. Details are also given by Olsen et al. (2017). The rise velocity is an important input to the mass transfer coefficient which governs gas dissolution.

The size of a bubble rising in water is governed by gas dissolution and gas expansion. Mathematically, this can be expressed by

$$\dot{d}_b = \frac{d_b}{3}\left(\frac{\dot{m}_b}{m_b} - \frac{\dot{\rho}_b}{\rho_b}\right) \tag{3}$$

Here m_b is the total mass of all gas components in the bubble. The first term on the right-hand side represents mass transfer (i.e., gas dissolution) and the second term represents gas expansion due to reduced hydrostatic pressure. This expression assumes single bubbles or very dilute bubble plumes. Bubbles rising in a denser bubble plume (typically from a gas blowout) will be influenced by neighbor bubbles and turbulence. This requires a more advanced bubble size model (Olsen & Skjetne, 2016b). Bubbles in both dilute and dense plumes are exposed to both mass transfer and gas expansion. The gas expansion is a result of the compressible nature of gas; that is, the density increases with increasing pressure. At low pressures this is well described by the ideal gas law. However, at significant ocean depths nonideal effects become more predominant and this needs to be accounted for as shown by Olsen & Skjetne (2016a, 2016b). The pressure applied for the density calculation is the sum of the hydrostatic pressure and the Laplacian pressure (Leifer & Patro, 2002).

Gas dissolution is a mass transfer phenomenon and the mass transfer rate is directly influencing the bubble diameter as seen in equation (3). Note that a methane bubble will absorb N_2, O_2, and other gas species from the ocean. For bubbles close to the ocean surface this is significant. Thus, a bubble size model needs to account for multispecies mass transfer:

$$\dot{m}_b = \sum_i \dot{m}_i \tag{4}$$

where $\dot{m}_i$ is the mass transfer rate of species i. This also enables calculations on bubbles which are initially multicomponent (e.g., natural gas). With these equations, it is possible to make a numerical estimate of the bubble size evolution if an accurate prediction of the mass transfer rate is available. We apply a forward-Euler method with a time step which is sufficiently small to avoid numerical diffusion.

2.1. Mass Transfer

Mass transfer by dissolution is driven by the difference in solubility and background concentration. Mathematically, this is expressed by the Ranz-Marshall expression (Ranz & Marshall, 1952)

$$\dot{m}_i = A_b J_i = \pi d_b^2 \cdot k_i^l \cdot \left(c_i^{sol} - c_i^l\right) \tag{5}$$

where d_b is the bubble diameter (representing surface area), k_i^l is the mass transfer coefficient for species i in the surrounding liquid, c_i^{sol} is the solubility of species i in the surrounding liquid, and c_i^l is the concentration of

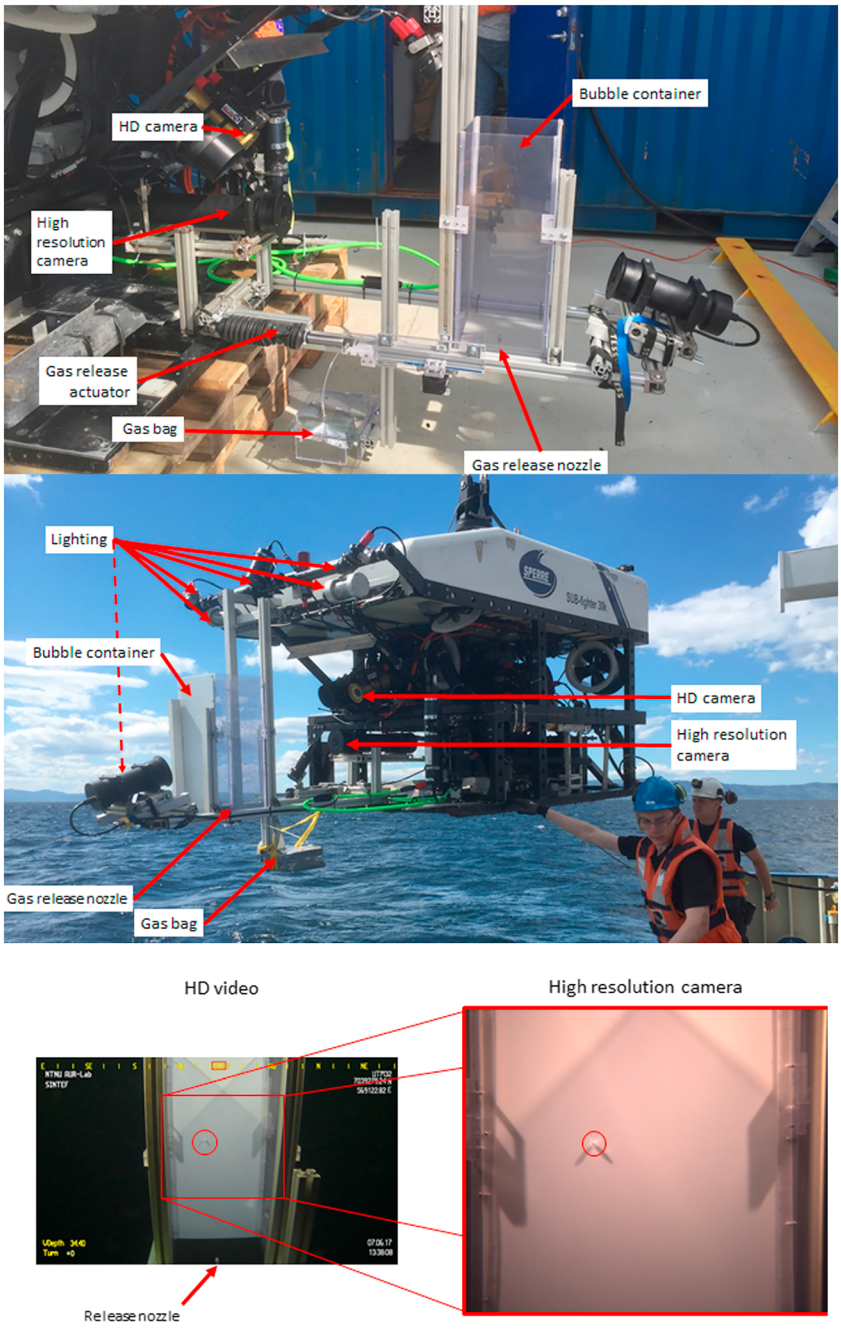

Figure 2. Images from the field experiment. Top image shows positioning of cameras, bubble container, and gas release mechanism. Middle image shows entire ROV, positioning of bubble equipment, and lightning. Bottom image shows examples of images from HD video camera and high-resolution camera. The location of the bubble is indicated by the red circle in the two images.

species *i* in the surrounding liquid (i.e., background concentration). The mass transfer coefficient quantifies how fast species are moving across an interphase (Olsen et al., 2017). Several mathematical expressions exist for the mass transfer coefficients. The coefficient is sensitive to variations in size and shape (spherical, ellipsoidal, spherical cap). The difference is also large between correlations that belong to different categories of surfactant level (contaminated, partly contaminated, or clean). There is also a slight difference between different correlations belonging to the same category. Several of these expressions are discussed elsewhere (e.g., Olsen et al., 2017). Here we focus on a few correlations.

Table 1
Analyzed Data Sets of Bubble Tracking

Data Set	Release Depth (m)	Final Depth (m)	Time (s)	Initial Diameter (mm)
1	300	107	850	5.6
2	100	35	284	6.5
3	100	83	71	6.0
4	300	187	505	5.7
5	200	80	530	4.5
6	200	125	310	5.8

For clean conditions we use the expression of Higbie (1935), which was theoretically derived and serves as an upper limit to mass transfer:

$$k = \frac{2}{\sqrt{\pi}}\sqrt{\mathrm{Re}\,Sc}\;\frac{D}{d_b} \tag{6}$$

Here *Re* and *Sc* is the Reynolds number and the Schmidt number, D is the diffusivity of the gas species in the surrounding liquid, and d_b is the bubble diameter. We consider two correlations for contaminated conditions (for reasons to become apparent further below). This is the correlation of Garner and Suckling (1958):

$$k = \left(2 + 0.95\cdot \mathrm{Re}^{1/2}Sc^{1/3}\right)\frac{D}{d_b} \tag{7}$$

and Frössling's (1938) correlation:

$$k = \left(2 + 0.6\cdot \mathrm{Re}^{1/2}Sc^{1/3}\right)\frac{D}{d_b} \tag{8}$$

The correlation by Frössling (1938) is derived for rigid spherical bubbles and considered a lower limit for the mass transfer coefficient. Note that the correlation of Garner & Suckling was erroneously credited to Hughmark (1967) in the preceding study by Olsen et al. (2017). The correlation is listed in Hughmark's paper, but was not derived by Hughmark (1967). For partly contaminated water, the mass transfer will behave as for clean conditions for large bubbles and as for contaminated conditions for smaller bubbles. The exact bubble size for the transition will probably depend on the concentration of surfactants. Zheng and Yapa (2002) developed a correlation for partly contaminated conditions suggesting a smooth transition below 2-mm bubble diameter. This is consistent with Rehder et al.'s (2002) experiment indicating that seawater falls into the category of partly contaminated conditions. Note that all observations of Rehder et al. (2002) were on bubbles above 4 mm. The correlation of Zheng and Yapa is widely used in the community studying bubbles in the ocean (McGinnis et al., 2006). The difference between these correlations is illustrated in Figure 1. We see that clean conditions (Higbie, 1935) will give the highest mass transfer and contaminated conditions (Garner & Suckling, 1958; Frössling, 1938) the lowest mass transfer. Note that when performing calculations, the choice of drag laws must be consistent with the choice of mass transfer coefficient (e.g., when contaminated conditions are assessed both drag and mass transfer needs to be described with correlations for contaminated conditions).

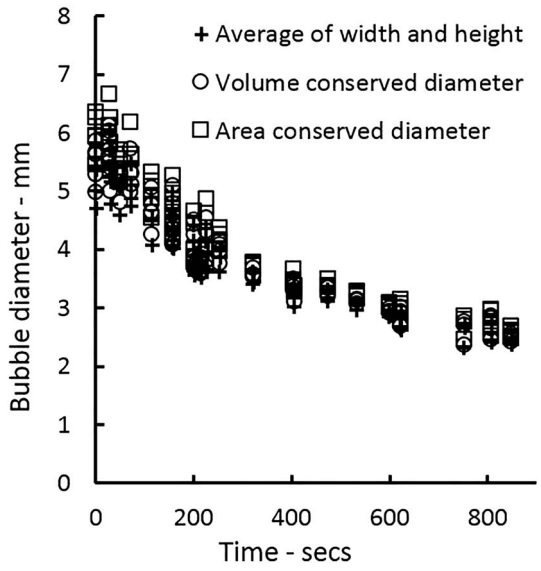

Figure 3. Estimated effective bubble diameter based on three different methods.

In order to calculate the mass transfer coefficient, the slip velocity between bubbles and water needs to be estimated since this is an input to the Reynolds number and the mass transfer coefficient. The slip velocity depends on buoyancy and drag by the following expression:

$$u_t = \sqrt{\frac{4}{3}\frac{g d_b}{C_D}\frac{\rho_l - \rho_b}{\rho_l}} \tag{9}$$

as shown elsewhere, for example, by Olsen et al. (2017). Here C_D is the drag coefficient which also depends on bubble size and concentration of surfactants. This is captured by the correlations for the drag coefficient derived by Tomiyama et al. (1998), which accounts for the bubbles shape and size and regime of contamination.

2.2. Field Experiment

The experimental configuration followed the concept of Rehder et al. (2002), by releasing individual gas bubbles at depth, and follow them as they rise. This required an ROV. We made use of NTNU's (Norwegian

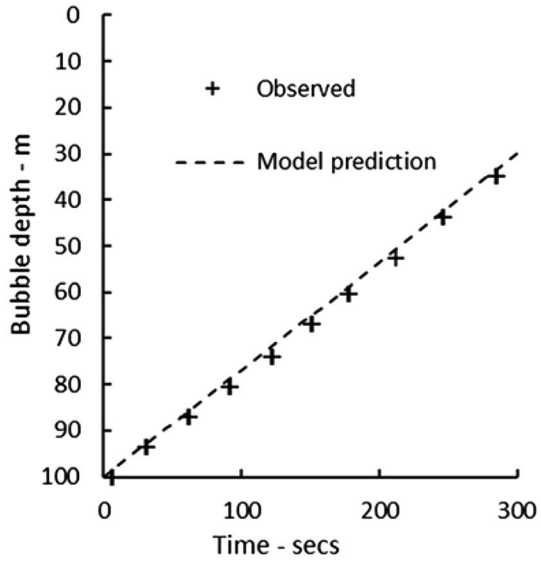

Figure 4. Model prediction of bubble rise compared to observed bubble rise.

University of Science and Technology) Subfighter 30 k from Sperre AS, which was operated by the NTNU AUR-Lab. To follow the bubble required careful adjustments of the ROV rise velocity (about 30 cm/s) by a skilled pilot. The bubble itself was released at depth into a clear Plexiglas box with a width of 294 mm, depth of 250 mm, and height of 643 mm. The box had a white back panel and an open top and bottom. This box was used to prevent the horizontal movement of the bubble from cross currents. Figure 2 shows photographs of the primary components of the experimental setup.

The release of methane (100% CH_4) bubbles into the base of the imaging cell was accomplished by remotely advancing a linear actuator that slowly turned a peristaltic pump via a rack and pinion. A collapsible gas bag was utilized to hold the supply of methane gas. A flexible tube connected the gas bag to the nozzle while passing through the peristaltic pump head. This method of dosing allowed a release of multiple millimeter methane bubbles. After releasing methane bubbles, the release nozzle was subsequently purged of gas by partially retracting the linear actuator so that gas expansion during the rise of the ROV would not continue to release additional methane gas bubbles. Although multiple bubbles were released in some instances, the bubble trajectories recorded for analysis had enough distance to neighboring bubbles to neglect bubble-bubble interactions.

Two camera systems were used to document the experiments: an HD video camera, with a field of view that covered the majority of the height of the Plexiglas box, from the release nozzle to just below the top opening. This camera was primarily used by the ROV pilot to adjust the vehicle rise velocity according to the rising bubble motion. A second, higher-resolution camera, with a smaller field of view, was used to document the bubble size over time during the experiment. This higher resolution was necessary to size the bubbles accurately. The high-resolution camera recorded uncompressed images of 2,448 × 2,048 pixels at 5 Hz with a pixel size of 0.14 mm.

The experiments were performed in Trondheimsfjord at a location with the following coordinates: 63.4990186°N, 10.2926071°E. The depth at the location was approximately 400-m water depth and very little cross-current was observed. CTD profiles were obtained multiple times during the day on which the data were collected. Little variation with time was observed. In principle we can assume a water temperature of 8 °C, salinity of 35 ppt and that O_2 was in equilibrium with the atmosphere. N_2 content was not measured. Since O_2 was in equilibrium with the atmosphere, it is reasonable to assume the same for N_2.

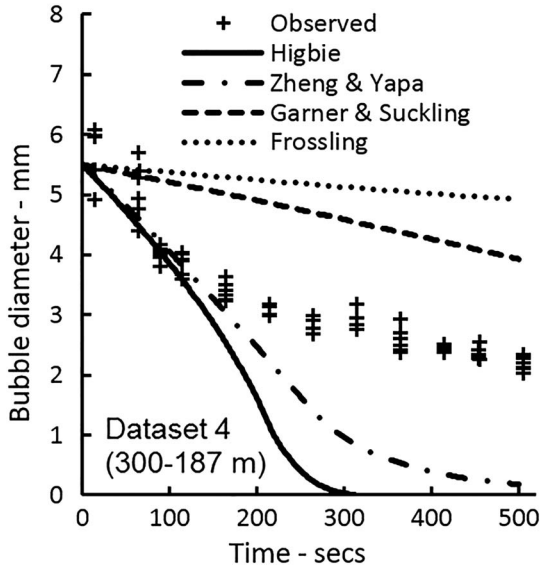

Figure 5. Observed and numerically estimated bubble diameter for data set 4. Numerical estimates apply different correlations for the mass transfer coefficient as indicated by the legend.

3. Results and Analysis

A total of six data sets were analyzed. These are summarized in Table 1.

The images recorded were analyzed by manual annotation in the open-source image processing software ImageJ (https://imagej.net). Due to the illumination used to image the bubbles, which included two lights angled downward from either side, the boundary of the bubble would vary along its perimeter from being illuminated (brighter than the background) or not directly illuminated (darker than the background). Given this variance of illumination and relative brightness compared to the background, the yet still distinct boundary (perimeter) of the bubble depicted in the images was manually traced using a Wacom DTZ-1200 W/G digitizing pad. This was conducted by personnel that have significant experience conducting similar biometry measurements using the same equipment. The width and height of bubbles were extracted. This

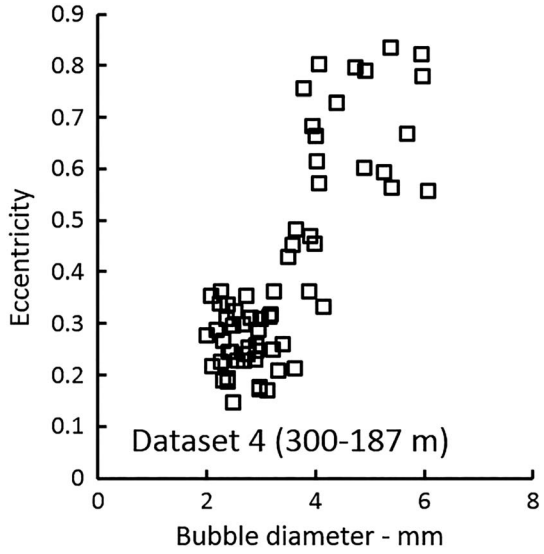

Figure 6. Bubble eccentricity calculated from measured width and height of bubbles as function of effective bubble diameter for data set 4.

was used to estimate the effective bubble diameter. The diameter of an oblate bubble can be calculated based on different approaches. We tested the following three methods:

1. the average of the width and height of the bubble,
2. calculate a total bubble volume based on width and height of an oblate spheroid and obtain the diameter of that volume for a sphere, and
3. calculate a total bubble surface area based on width and height of an oblate spheroid and obtain the diameter of that area for a sphere.

These methods are compared in Figure 3 for data set 1, which shows seemingly small differences between approaches. In the following figures and analyses we report the volume conserved bubble diameter (method 2) as the effective diameter. Wang and Socolofsky (2015) also discuss bubble size quantification from image analysis.

The depth of the bubbles as a function of time was also recorded. This relates to the rise velocity. A comparison between observed and theoretical progression of bubble depth is seen in Figure 4 for data set 2. The comparison shows that there is very good consistency between theory and observations. This indicates that the chosen drag law represents the conditions of the experiment. It should also be noted that there is no difference between drag laws for clean, partly contaminated, and contaminated conditions. This is as expected, since only smaller bubbles should be sensitive to this (Clift et al., 1978). Typical rise velocities are 22–24 cm/s. It should also be noted that the validation is only for bubbles above 3 mm. There are no observations in this experiment to support the model for smaller bubbles. However, the model was validated for smaller bubbles in contaminated conditions in an earlier experiment (Olsen et al., 2017).

When comparing theory with observations of bubble size evolution, the situation becomes more complex. This is shown for data set 4 in Figure 5. Note that the full data set of recorded images cannot be shown here as this would only appear as a cloud of points due the high frequency of image acquisition. Instead, data points are shown in an appropriate time interval with roughly five data points from consecutive images. These five data points indicate the average value and variations which can be attributed to bubble oscillations (wobbly behavior). There is no good match between observed bubble size evolution and bubble size evolution estimated by theory for all mass transfer correlations investigated. Initially, there seems to be a reasonable match between observations and theory if a correlation for clean (Higbie, 1935) or partly contaminated (Zheng & Yapa, 2002) conditions are applied. However, these also deviate from observations when the bubble shrinks below 4 mm. When further studying the curve for observed bubble size, for data set 4 and the other data sets (see below), there seems to be a transition between bubble diameters of roughly 3 and 4 mm. Bubbles above 4 mm shrink faster than bubbles below 3 mm. We believe that this can explained by a shift in bubble shape.

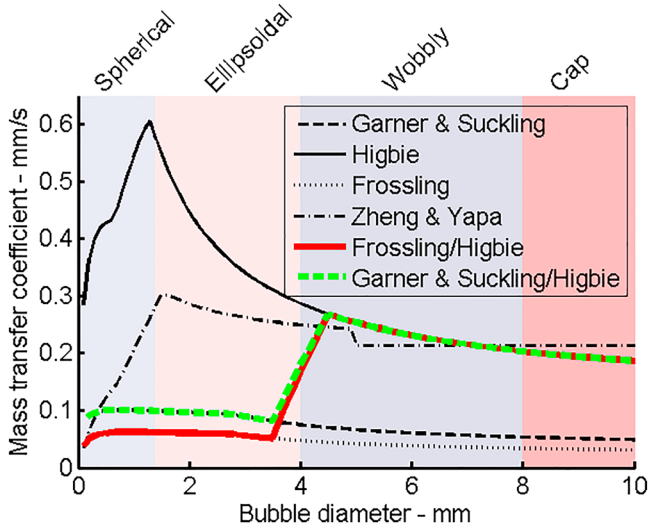

Figure 7. New correlations for drag coefficient plotted on top of an approximate phase diagram indicating bubble shape/behavior.

Bubble eccentricity is a measure of deviation from a spherical shape. For a spherical particle, the eccentricity is equal to zero. Figure 6 shows that eccentricity increases with bubble size and that there is a marked change in eccentricity between 3 and 4 mm. Both Clift et al. (1978) and Bhaga and Weber (1981) categorized the shift between 3 and 5 mm as a shift from ellipsoidal bubbles to a regime they named *wobbly* bubbles. The so-called wobbly behavior refers to oscillations which enhances mass transfer. Based on this we propose that bubbles observed in the experiment changes behavior with respect to mass transfer between 3 and 4 mm. The larger bubbles behave more as clean bubbles and smaller bubbles more as contaminated bubbles.

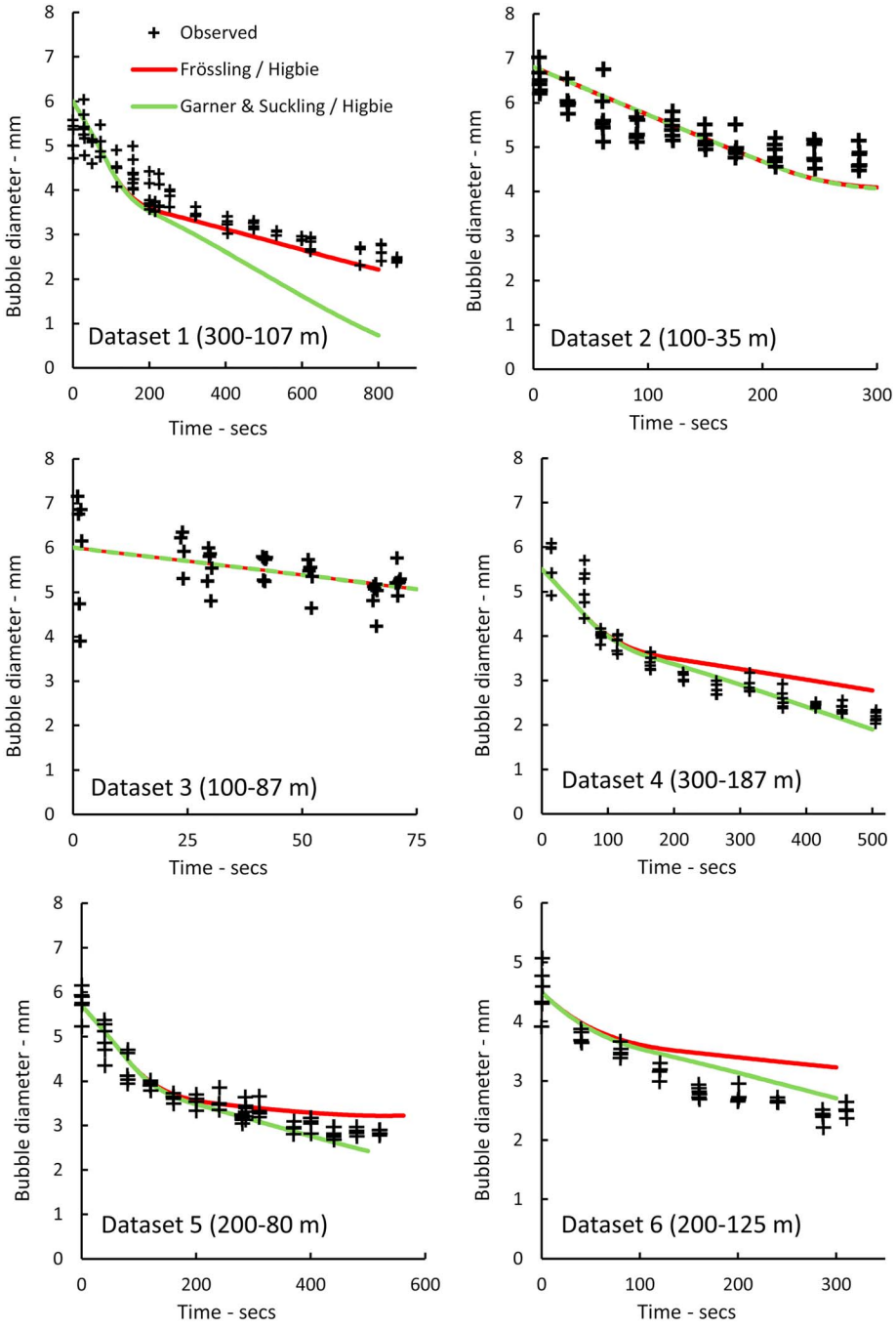

Figure 8. New mass transfer correlations compared with experimental observations.

Two new correlations for mass transfer are proposed which we name *Frössling/Higbie* and *Garner & Suckling/Higbie*. Both use an expression for the contaminated condition for bubbles below 3.5 mm and an expression for clean bubbles above 4.5 mm. Between 3.5 and 4.5 mm there is a linear transition between contaminated and clean conditions. Both new correlations assume Higbie's (1935) correlation for the clean regime. The *Frössling/Higbie* correlation assumes Frössling's (1938) expression for the contaminated regime and *Garner & Suckling/Higbie* correlation assumes Garner and Suckling's (1958) expression for the contaminated regime. These are plotted in Figure 7. Note that these share some of the same principles as the correlation of Zheng et al. (2003) with a transition from contaminated to

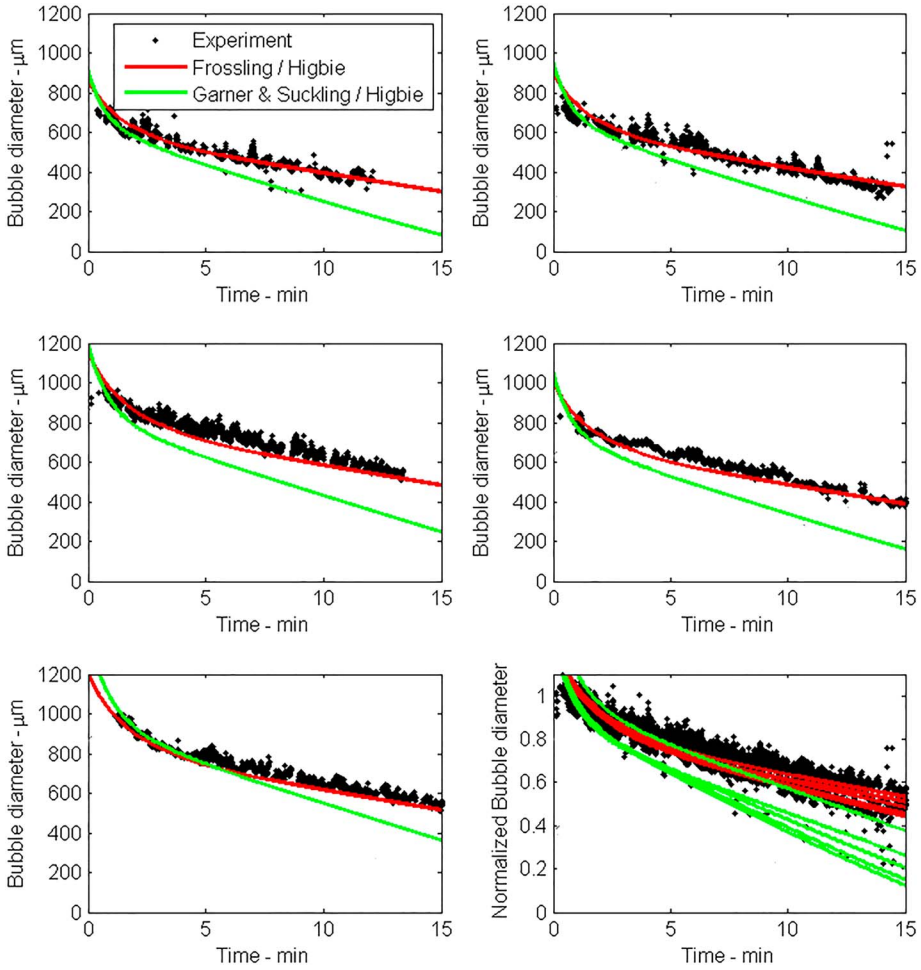

Figure 9. Bubble size evolution for five inverted cone experiments with small bubbles (Olsen et al., 2017). Note that bottom right plot is a summary of all five experiments with a normalized bubble size along the *y* axis.

clean conditions with increasing bubble size. However, the shift is placed at a higher bubble size for the new correlations. These correlations are categorized as correlations for partly contaminated conditions.

When applying these new correlations in the theoretical model for bubble size evolution, the consistency with the experimentally observed bubble size evolution is good. This is shown in Figure 8. The performance of these correlations is significantly better than the previously tested correlations. For data sets 2 and 3 both new correlations give equally good consistency with experimental observations. For data set 1, the Frössling/Higbie correlation has the best fit with measurements, while for data sets 4, 5, and 6 the Garner & Suckling/Higbie correlation has the best fit.

4. Comparison With Other Experiments

The above comparison between the observations from the field experiment in the Trondheimsfjord with new correlations for mass transfer indicates that the new correlations can describe the experiments fairly well. These correlations are more robust than earlier correlations since they are based on experimental data which span a wider range of bubble sizes, from 2 to 7 mm. Note that more effects can still be studied, that is, wider ranges of initial bubble sizes and ocean locations with various surfactant content. That might motivate future experiments. Meanwhile it is worthwhile to compare the proposed correlations with earlier experiments.

Olsen et al. (2017) performed experiments in the lab in an inverted cone bubble column where water was pumped in from the sea through a pipe. The initial bubble size was typically 1 mm. The old analysis

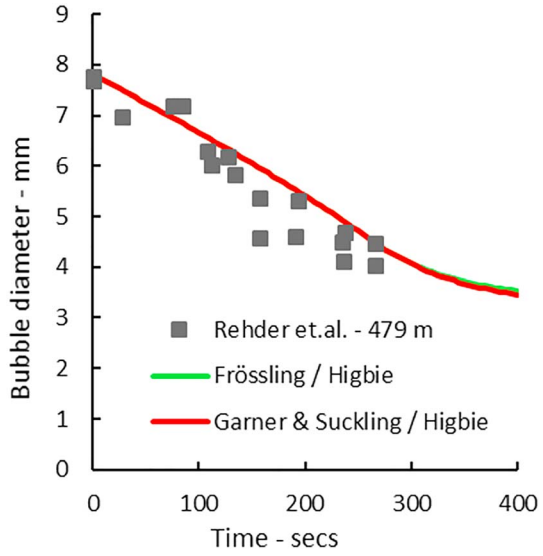

Figure 10. Bubble size evolution for a large bubble in the Monterey Bay released from 479-m depth.

(Olsen et al., 2017) concluded that Garner & Suckling's mass transfer correlation gave the best fit between theory and experiments. There was an overestimate of the initial bubble size in the first analyses, which to some degree influences this interpretation. When more carefully estimating the initial bubble size and applying the new correlations suggested above in the numerical model, we find quite good consistency between theory and experiments as indicated in Figure 9. This is particularly true for the Frössling/Higbie correlation which is somewhat better than Garner & Suckling/Higbie. For more details on this analysis and the data set we refer to Olsen et al. (2017).

Rehder et al. (2002) tracked methane bubbles by a camera mounted on an ROV in the Monterey Bay. They only observed bubbles above 4 mm. When comparing with these experiments, both new correlations behave very similar and both are consistent with the experiment as seen in Figure 10. This is as expected since the correlations are equal for bubble sizes above 4 mm. Thus, the proposed new correlations for the mass transfer coefficient seem to be fairly consistent with both new and earlier experiments on gas dissolution in seawater.

5. Conclusions

New data sets of bubble size evolution due to gas dissolution and gas expansion in the ocean have been obtained by releasing, tracking, and filming methane bubbles with an ROV in the Trondheimsfjord. Released bubbles had an initial diameter between 5 and 7 mm and were tracked until they reached a diameter of roughly 2 mm.

The new data sets were compared against theory, applying established correlations for the mass transfer coefficient. There was an inconsistency between experiment and theory. Thus, new correlations for the mass transfer were proposed. The new correlations are consistent with the new experiments and previously published experiments. The new correlations introduce a transition in mass transfer behavior between 3.5 and 4.5 mm. For bubbles smaller than 3.5 mm an expression for contaminated conditions are applied and for bubbles larger than 4.5 mm an expression for clean conditions are applied. We have chosen Higbie (1935) correlation for clean bubbles and Frössling's (1938) and Garner and Suckling (1958) correlations for dirty contaminated bubbles. Other correlations might be assessed, but here we focus on the importance of acknowledging a transition between clean and contaminated conditions at roughly 3.5 to 4.5 mm. Of the new correlations, the Frössling/Higbie correlation is very consistent with 9 out of 12 experiments, and the Garner & Suckling/Higbie correlation is very consistent with 6 out of 12 experiments. The Frössling/Higbie correlation is the most conservative correlation (i.e., estimates the lowest mass transfer).

The new correlations represent a contamination regime often referred to as partly contaminated with a transition between clean and contaminated conditions around 3.5 to 4.5 mm. It is observed in general that in almost all contaminated conditions the bubbles will behave as clean if the bubble size becomes sufficiently large, typically above 7–8 mm (Clift et al., 1978). The new correlations for seawater presented her represent a contamination regime which might be referred to as partly contaminated with a transition between clean and contaminated conditions around 3.5 to 4.5 mm. Others also come to the same conclusion for seawater (e.g., Leifer & Patro, 2002; McGinnis et al., 2006). It has also been proposed that the shift may move to higher bubble sizes as the concentration of surfactants increases (Alves et al., 2005). Thus, a shift might be observed at even higher bubble sizes. Further investigations should be pursued.

Acknowledgments
The authors would like to acknowledge the financial support from the partners in the SURE project: Total, Statoil, Wild Well, and Petroleum Safety Authority Norway. We would also like to thank Pedro De La Torre and the NTNU AUR-Lab for the access to the ROV and for the excellent piloting, together with the crew from R/V *Gunnerus*. The data set is available in the supporting information.

References

(IPCC), I. P. o. C. C (2013). *Climate Change 2013: The Physical Science Basis. Contribution of Working Group I to the Fifth Assessment Report of the Intergovernmental Panel on Climate Change*. Cambridge, UK and New York: Cambridge University Press.

Alves, S. S., Orvalho, S. P., & Vasconcelos, J. M. T. (2005). Effect of bubble contamination on rise velocity and mass transfer. *Chemical Engineering Science*, *60*(1), 1–9. https://doi.org/10.1016/j.ces.2004.07.053

Aoki, J., Hayashi, K., Shigeo, H., & Tomiyama, A. (2015). Effects of surfactants on mass transfer from single carbon dioxide bubbles in vertical pipes. *Chemical Engineering and Technology*, *38*(11), 1955–1964. https://doi.org/10.1002/ceat.201500063

Bhaga, D., & Weber, M. E. (1981). Bubbles in viscous liquids: Shapes, wakes and velocities. *Journal of Fluid Mechanics*, *105*(1), 61–85. https://doi.org/10.1017/S002211208100311X

Clift, R., Grace, J. R., & Weber, M. E. (1978). *Bubbles, drops, and particles*. New York, London: Academic Press.

Frössling, N. (1938). Über die Verdunstung falender Tropfen. *Gerlands Beitraege zur Geophysik*, *52*, 170–216.

Garner, F. H., & Suckling, R. D. (1958). Mass transfer from a soluble solid sphere. *AICHE Journal*, *4*(1), 114–124. https://doi.org/10.1002/aic.690040120

Higbie, R. (1935). The rate of absorption of a pure gas into a still liquid during short periods of exposure. *Transactions of the A.I.Ch.E.*, *31*, 365–389.

Hughmark, G. A. (1967). Liquid-liquid spray column drop size, holdup, and continuous phase mass transfer. *Industrial and Engineering Chemistry Fundamentals*, *6*(3), 408–413. https://doi.org/10.1021/i160023a014

Laqua, K., Malone, K., Hoffmann, M., Krause, D., & Schlüter, M. (2016). Methane bubble rise velocities under deep-sea conditions—Influence of initial shape deformation. *Colloids and Surfaces A: Physicochemical and Engineering Aspects*, *505*, 106–117. https://doi.org/10.1016/j.colsurfa.2016.01.041

Leifer, I., & Patro, R. K. (2002). The bubble mechanism for methane transport from the shallow sea bed to the surface: A review and sensitivity study. *Continental Shelf Research*, *22*(16), 2409–2428. https://doi.org/10.1016/S0278-4343(02)00065-1

McGinnis, D. F., Greinert, J., Artemov, Y., Beaubien, S. E., & Wüest, A. (2006). Fate of rising methane bubbles in stratified waters: How much methane reaches the atmosphere? *Journal of Geophysical Research*, *111*, C09007. https://doi.org/10.1029/2005JC003183

Olsen, J. E., Dunnebier, D., Davies, E. J., Skjetne, P., & Morud, J. (2017). Mass transfer between bubbles and seawater. *Chemical Engineering Science*, *161*, 308–315. https://doi.org/10.1016/j.ces.2016.12.047

Olsen, J. E., & Skjetne, P. (2016a). Current understanding of subsea gas release—A review. *Canadian Journal of Chemical Engineering*, *94*(2), 209–219.

Olsen, J. E., & Skjetne, P. (2016b). Modelling of underwater bubble plumes and gas dissolution with an Eulerian-Lagrangian CFD model. *Applied Ocean Research*, *59*, 193–200. https://doi.org/10.1016/j.apor.2016.06.001

Pakulski, J. D., & Brenner, R. (1994). Abundance and distribution of carbohydrates in the ocean. *Limnology and Oceanography*, *39*(4), 930–940. https://doi.org/10.4319/lo.1994.39.4.0930

Ranz, W. E., & Marshall, W. R. J. (1952). Evaporation from droplets, parts I & II. *Chemical Engineering Progress*, *48*, 173–180.

Rehder, G., Brewer, P. W., Peltzer, E. T., & Friedrich, G. (2002). Enhanced lifetime of methane bubble streams within the deep ocean. *Geophysical Research Letters*, *29*(15), 1731. https://doi.org/10.1029/2001GL013966

Rehder, G., Leifer, I., Brewer, P. G., Friedrich, G., & Peltzer, E. T. (2009). Controls on methane bubble dissolution inside and outside the hydrate stability field from open ocean field experiments and numerical modeling. *Marine Chemistry*, *114*(1–2), 19–30. https://doi.org/10.1016/j.marchem.2009.03.004

Ruppel, D. R., & Kessler, J. D. (2017). The interaction of climate change and methane hydrates. *Reviews of Geophysics*, *55*, 126–168. https://doi.org/10.1002/2016RG000534

Sabbaghzadeh, B., Upstill-Goddard, R. C., Beale, R., Pereira, R., & Nightingale, P. D. (2017). The Atlantic Ocean surface microlayer from 50°N to 50°S is ubiquitously enriched in surfactants at wind speeds up to 13ms1. *Geophysical Research Letters*, *44*, 1–7. https://doi.org/10.1002/2017GL072988

Takemura, F., & Yabe, A. (1999). Rising speed and dissolution rate of a carbon dioxide bubble in slightly contaminated water. *Journal of Fluid Mechanics*, *378*, 319–334. https://doi.org/10.1017/S0022112098003358

Tomiyama, A., Kataoka, I., Zun, I., & Sakaguchi, T. (1998). Drag coefficients of single bubbles under normal and micro gravity conditions. *JSME International Journal, Series B*, *41*(2), 472–479. https://doi.org/10.1299/jsmeb.41.472

Wang, B., & Socolofsky, S. A. (2015). A deep-sea, high-speed, stereoscopic imaging system for in situ measurement of natural seep bubble and droplet characteristics. *Deep Sea Research Part I: Ocenographic Research Papers*, *104*, 134–148. https://doi.org/10.1016/j.dsr.2015.08.001

Wang, B., Socolofsky, S. A., Breier, J. A., & Seewald, J. S. (2016). Observations of bubbles in natural seep flares at MC 118 and GC 600 using in situ quantitative imaging. *Journal of Geophysical Research: Oceans*, *121*, 2203–2230. https://doi.org/10.1002/2015JC011452

Zheng, L., & Yapa, P. D. (2002). Modeling gas dissolution in deepwater oil/gas spills. *Journal of Marine Systems*, *31*(4), 299–309. https://doi.org/10.1016/S0924-7963(01)00067-7

Zheng, L., Yapa, P. D., & Chen, F. H. (2003). A model for simulating deepwater oil and gas blowouts—Part I: Theory and model formulation. *Journal of Hydraulic Research*, *41*(4), 339–351. <Go to ISI>://000184971700001